Final Technical Report

University of Utah

DOE Grant Number: DE-FG02-03ER46086

Project Title: Thermodynamic, Kinetic and Electrochemical Studies on Mixed Proton, Oxygen Ion and Electron (Hole) Conductors

Period of Performance: September 1, 2015 to August 31, 2021.

PI: Prof. Anil V. Virkar
Phone: (801) 581-5396
Email: anil.virkar@utah.edu

Table of Contents

Final Report

II(a): Scope of Originally Proposed Work and any Changes: The principal objective of the work was to conduct thermodynamic, kinetic and electrochemical studies on mixed proton, oxygen ion and electron (hole) conductors. The project also involved studies on cation conductors such as Li^+ and Na^+ ion conductors of particular relevance to batteries. The work involved theory and experiments. Since any use of ionic conductors necessarily entails two electrodes, electrode reactions are central to the overall transport processes from one electrode, through the electrolyte, to the other electrode. The role of interfaces and electrochemical reactions is thus of central importance. Transport processes in fuel cells, electrolyzers, lithium batteries and sodium batteries were examined using linear non-equilibrium thermodynamics, which is based on the assumption of small departures from thermodynamic equilibrium. The main approach involved expressing transport processes using the Onsager equations which naturally include coupling of thermodynamic flows and thermodynamic forces. The basic tenet of linear non-equilibrium thermodynamics is the existence of *local thermodynamic equilibrium* which means that all thermodynamic functions are locally defined [1-3]. Thus, chemical potentials of various species are defined locally as a function of position and also of time. The existence of local thermodynamic equilibrium has fundamental implications concerning transport of electronic species through a predominantly ionic conductor. For instance, in *steady state*, local equilibrium in an oxygen ion conductor implies that the reaction $\frac{1}{2}O_2 + 2e' \rightarrow O^{2-}$ is locally (at $\vec{r}$) in equilibrium [4]. This further means that $\frac{1}{2}\mu_{O_2}(\vec{r}) + 2\tilde{\mu}_e(\vec{r}) = \tilde{\mu}_{O^{2-}}(\vec{r})$ and $\frac{1}{2}\delta\mu_{O_2}(\vec{r}) + 2\delta\tilde{\mu}_e(\vec{r}) = \delta\tilde{\mu}_{O^{2-}}(\vec{r})$ inside the electrolyte in which $\mu_{O_2}(\vec{r})$ is the chemical potential of neutral oxygen gas, $\tilde{\mu}_e(\vec{r})$ is the electrochemical potential of electrons and $\tilde{\mu}_{O^{2-}}(\vec{r})$ is the electrochemical potential of oxygen ions. The δ's denote small variations (differentials). It has been previously demonstrated that chemical potential of gaseous O_2 is well-defined inside a fully dense solid electrolyte [4]. The implication thus is that for small changes (fluctuations) to occur in these thermodynamic potentials, in addition to finite nonzero oxygen ion conductivity, the electronic conductivity must also be finite nonzero, however small it may be. If the ionic transference number is say 0.9999, it means the electronic conductivity is four orders of magnitude smaller than the ionic conductivity – but is not zero [4]. This small electronic conductivity has negligible effect on Faradaic efficiency. Thus, the measured external current for an electrochemical device is essentially that corresponding to ionic flow through the electrolyte. The electronic conductivity, however, has a large effect on the chemical potential of oxygen, μ_{O_2}, in the electrolyte. The chemical potential of oxygen plays a vital role in thermodynamic and mechanical stability of the electrolyte. The overall transport through electrolytes is fundamentally governed by the Onsager transport equations. The flux of species *i* is related to the gradients of various chemical potentials by [1-3]

$$j_i = -\sum_j L_{ij}\nabla\mu_j \qquad (1)$$

where L_{ij} are the Onsager coefficients. For a mixed proton, oxygen ion and electron (hole) conductor, the relevant coefficients are $L_{H_2H_2}, L_{O_2O_2}$ and $L_{O_2H_2}$, and the forces are $-\nabla\mu_{H_2}$ and $-\nabla\mu_{O_2}$ [5]. These coefficients for a fuel cell or an electrolyzer based on a mixed proton, oxygen ion and electron (hole) conductor can be completely described in terms of ionic conductivities (for both O^{2-} and H^+), electronic conductivity (however small), specific electrode polarization resistances (for both electrodes), specific resistances for transport of electrons/holes across electrolyte/electrode interfaces, both electrode reactions, that is $\frac{1}{2}O_2 + 2e' \leftrightarrow O^{2-}$ and $\frac{1}{2}H_2 \leftrightarrow H^+ + e'$, and including the externally applied load [5]. The theoretical work demonstrated that small changes in electronic conductivity can induce large changes in μ_{O_2} and μ_{H_2} inside the electrolyte as well as at the electrolyte/electrode interfaces. The theoretical work on lithium ion batteries, which are prone to forming lithium metal dendrites, also shows that very small changes in electronic transport through the electrolyte (however small may be the electronic conductivity) can substantially change the chemical potential of lithium, μ_{Li}, which is central to forming dendrites [6]. The same logic applies to all ionic conductors (solid or even gel type) capable of transporting multiple species. Ultimately, the key result is that the sign of the Onsager cross coefficients, L_{ij} for $i \neq j$ depends

on the relative directions of ionic and electronic currents flowing through the electrolyte [5,6]. If the ionic and the electronic currents are *anti-parallel*, then $L_{ij} > 0$. In such cases, the chemical potentials of all neutral species (e.g. μ_{H_2} and μ_{O_2}) in the electrolyte are mathematically bounded by the electrode values. If, however, ionic and electronic currents are *parallel*, then $L_{ij} < 0$. Under such conditions, the chemical potentials of the neutral species inside the electrolyte need not be mathematically bounded by the electrode values. If either μ_{H_2} and/or μ_{O_2} exceed thermodynamic/mechanical stability limits of the electrolyte, the membrane and as a result the electrochemical device can degrade [5,6]. The observed degradation of electrolyzers and degradation of lithium batteries (and sodium batteries) has origin in Onsager equations and linear non-equilibrium thermodynamics. It is to be emphasized, however, that there are many other reasons for electrochemical devices to fail. The main result of our work is that there are fundamental thermodynamic reasons which determine the stability of electrochemical systems [5-7].

II(b): Introduction: Ionic conductivity of an electrolyte is clearly of central importance in an electrochemical device/system. There are numerous reported studies on various ionic conductors for this reason. Limited work is reported on electronic conductivity of ionic conductors. However, yttria-stabilized zirconia (YSZ) is one of the solid electrolytes on which many studies on the measurement of electronic conductivity have been reported [8,9]. The most common approach has been the use of Hebb-Wagner polarization method. In the typical Hebb-Wagner method, the sample is polarized under a large applied voltage [10,11]. This results in large chemical potential gradients in the sample. For the aforementioned reasons of electrolyte stability and non-equilibrium thermodynamics, the measurement of electronic conductivity under well-defined conditions in solid electrolytes is deemed important. We have conducted theoretical and experimental work on the measurement of electronic conductivity of predominantly ionic conductors [12,13]. In order to obtain absolute values of the electronic conductivity, the methods developed in this work involved very small applied voltage/chemical potential differences. Electrochemical impedance spectroscopy (EIS) is routinely used to determine electrolyte conductivity and electrode polarization resistances. Often, however, deconvolution of EIS spectra is difficult – as multiple equivalent circuits give essentially identical spectra. As a result, the inverse problem of determining cell parameters from the measured EIS spectra is not unique. We have addressed this aspect in our work in two ways: (a) The measurement of electrode polarization on a model system using a DC method. Since the method is DC, it does not include capacitances (or constant phase elements) in the equivalent circuits used to analyze data. (b) Embedded screen probes. This approach actually uses EIS. But spectra are obtained between the screen probe and the two electrodes (cathode and anode) separately, as well as across the cathode and the anode. This approach allows one to separately determine polarizations of the two electrodes. Many solid electrolytes, YSZ in particular, exhibit grain-size dependent conductivity. Grain boundaries are generally more resistive than grains. It has been known for a long time that this can be attributed to space charge effects [14,15]. Detailed analysis of space charge in sodium chloride was given by Kliewer and Koehler [16]. The analysis reported to date for YSZ, however, was based on a simpler approach which assumed all defects in equilibrium [14,15]. We have recently conducted detailed analysis of space charge in YSZ, which takes into account defect complexes, and does not assume the dilute limit (deviation from the Boltzmann distribution) [17]. The work, also takes into account response of oxygen vacancies to 'frozen-in' cation defects. This replicates the real situation in that most O^{2-} ion transporting solid electrolytes are fabricated at high temperatures (where cations are mobile) but are used at lower temperatures where cations are frozen (essentially immobile).

II(c):1: A Parametric Model for Solid Oxide Fuel Cells (SOFC) based on Out of Cell Measurements: A typical anode-supported solid oxide fuel cell has the following components: (i) Anode support, (ii) Anode functional layer, (iii) Electrolyte, (iv) Cathode functional layer, and (v) Cathode current collector. All these are independent components (since their compositions, porosities, thicknesses can be independently selected) with their different properties. A minimum number of parameters needed to model SOFC performance are nine. They are: (a) Effective gas diffusivities for the four porous layers (anode support,

anode functional layer, cathode functional layer, and cathode current collector) – that is (4). (b) Activation polarization at the cathode (exchange current density and transfer parameter) (2), and activation polarization at the anode (2). (c) Ohmic contribution from the electrolyte, electrode layers and interfaces. The experimentally measured voltage vs. current density curves are, however, are very simple in shape – requiring no more than 2 or 3 independent 'fitting' parameters using a polynomial fit. This means, at the most one can determine 2 or 3 of the 9 parameters from the polynomial fit. This also means in actuality, it is not possible to determine virtually any of the real parameters from the measured voltage-current density data *uniquely* because of the inverse nature of the problem. The same thing is true of EIS also, in that it is not possible to obtain a set of unique parameters by fitting to EIS spectra. We have developed a parametric model based on out-of-cell (and some in-cell) parameters that can be actually measured. This approach is thus different since it is a solution to a forward problem; determination of how the cell will perform based on model parameters that can actually be measured. The paper also shows that fundamental parameters such as exchange current density, can be deduced from the coefficients of the polynomials. A paper based on this work was published in *J. Power Sources* (2015) [18].

II(c):2: Measurement of Electronic Conductivity of 8YSZ by a Transient Technique: We have developed a new oxygen permeation technique to measure the electronic conductivity of YSZ. The permeation cell is a YSZ disc with an embedded Pt probe and a cavity at the center (Figure 1 shows a schematic of the approach) [13]. By applying a small DC bias (0.03V), oxygen is pumped into the YSZ disc and stored in the cavity. In steady state, a stable Nernst potential is developed between the cavity and the outer surfaces. The Nernst voltage is very close to the applied voltage since YSZ is essentially an ionic conductor. When the DC bias is removed, oxygen permeates out of the cavity leading to a decay of the Nernst potential. Electronic conductivity of YSZ corresponding to the ambient oxygen pressure (~0.21 atm) is determined by analyzing the time dependence of the decay of Nernst potential. This approach is a variation of our previous paper [12], with one important difference. The YSZ disc has an isolated cavity of known volume. Thus, the actual

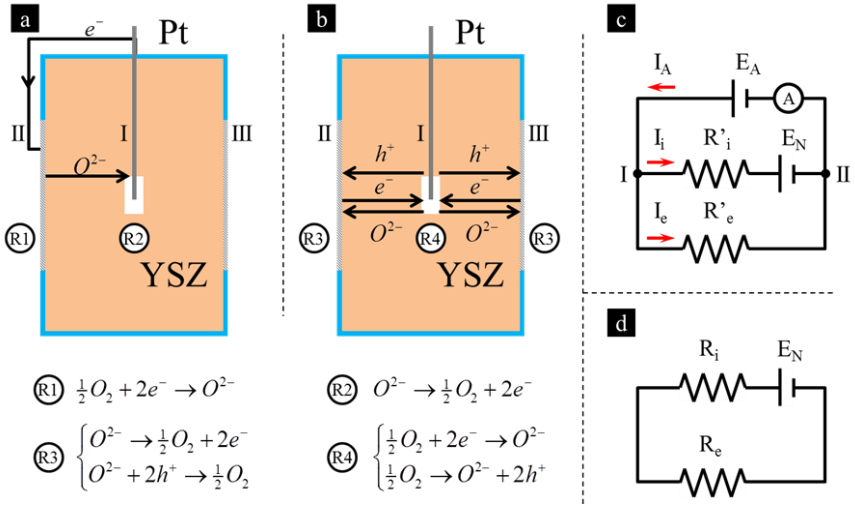

Figure 1: A schematic cross-sectional view of a 8YSZ disc sample with an embedded Pt probe (grey line) and a cavity (white region). a) The charge migration path and electrode reactions (R1 and R2) during the charging stage. The blue border is an impervious glass coating. b) The charge migration paths and electrode reactions (R3 and R4) during the discharging stage. c) The equivalent circuit describing the charging stage. d) The equivalent circuit describing the discharging (permeation) stage.

amount of oxygen pumped into the cavity can be precisely calculated. The application of a very small voltage also means that there is virtually no change in the stoichiometry of 8YSZ, unlike the case when using the Hebb-Wagner method [10,11]. Using the same experiment, we were also able to determine the ionic conductivity of 8YSZ. A paper based on this work was published in *J. Power Sources* (2016) [13].

II(c):3: Nanocathodes by a Solution Spray Process: Typical SOFC cathodes consist of single phase mixed ionic-electronic conducting (MIEC) oxides or composites of an electronic conducting or MIEC oxide and an oxygen ion conductor. These are usually heated to as high as 1150^{o}C during cathode firing. The objective of the present work was to synthesize single phase MIEC and MIEC + oxygen ion conductor composites using a low temperature spray-pyrolysis process by direct deposition on electrolyte/anode support sintered discs [19]. Composite nano-cathodes containing Sr-doped $LaMnO_3$ (LSM) and Gd_2O_3-doped CeO_2 (GDC) were deposited on yttria-stabilized zirconia (YSZ) discs and YSZ/NiO + YSZ bi-layer discs using an aqueous solution. The samples were heated over a range of temperatures from 700^{o}C to 1200^{o}C to form LSM + GDC porous films. The crystallite size was estimated using X-ray diffraction (XRD) Scherrer formula. The crystallite size was in the ~3 nm to ~80 nm range. Polarization resistance was measured by electrochemical impedance spectroscopy (EIS) from 400^{o}C to 700^{o}C. Nano-cathodes of ~70 nm thickness fired at 700^{o}C exhibited polarization resistance of ~0.23 Ωcm^2 at 700^{o}C. Fuel cell tests were conducted at 700^{o}C on cells with nano-cathodes and a conventional LSM + YSZ cathode. The maximum power density was ~0.51 Wcm^{-2} with nano-cathodes. By contrast, the corresponding power density with conventional LSM + YSZ cathodes was ~0.11 Wcm^{-2}. This work showed that very thin cathode functional layers can be deposited on sintered YSZ/NiO + YSZ bi-layer discs by using an aqueous solution. This approach in principle can be extended to large area cells. Thus, in concept, cathode functional layer can be deposited on sintered electrolyte/anode support bi-layers. This may avoid the usual practice of firing cathode functional layer (applied by screen printing) to high temperatures (~1150^{o}C) and suppress the associated coarsening. A paper based on this work was published in *J. Electrochem. Soc*. (2016) [19]. Further work has also been conducted on a number single phase and composite cathodes. The measurement of their polarization resistance showed that the activation energies are about the same for all of these cathodes as shown in Figure 2. This is not surprising in that they all contain the same transition metals (Co, Fe, Mn), so the fundamentals of the oxygen reduction reaction (ORR) should be very similar. Large differences in the actual polarization resistances observed are attributed to the large differences in their microstructures.

II(c):4: Space Charge in 8YSZ: Role of Non-Equilibrium Defects Distributions: Space charge in 8YSZ was examined theoretically. The Poisson-Boltzmann equation was solved by free energy minimization. The Helmholtz free energy of a crystal containing various defects was minimized subject to two constraints: (1) The total dopant concentration is fixed and (2) the maximum amount of surface charge is limited by site density [17]. Large dopant concentration leads to defect concentrations which deviate from the Boltzmann distribution. When the free energy is minimized assuming all defects attain their equilibrium distributions, the corresponding electrochemical potentials are equilibrated through the crystal. These calculations correspond to long annealing times. From these calculations, it was demonstrated that electrochemical potentials of all species are equilibrated. For example, the electrochemical potential of oxygen vacancies, is given by $\tilde{\mu}_{\ddot{V}_O}(\text{surface}) = \tilde{\mu}_{\ddot{V}_O}(\text{bulk})$ and that of yttrium ions on zirconium sites is given by $\tilde{\mu}_{\acute{Y}_{Zr}}(\text{surface}) = \tilde{\mu}_{\acute{Y}_{Zr}}(\text{bulk})$. This means all species are equilibrated. The corresponding space charge potential was determined by solving the Poisson-Boltzmann equation. The same is the case for all other defects (and ions) provided equilibration of all species is assumed. This is the case when the temperature is high, a typical sintering temperature. However, YSZ is sintered at ~1500^{o}C, but is used at 800^{o}C or even lower. At low temperatures, the only mobile defects are oxygen vacancies. Free energy minimization was done at a lower temperature (e.g. 800^{o}C) after a high temperature heat treatment, such as at 1500^{o}C. At 800^{o}C, cation defects such as yttrium on zirconium site are essentially frozen corresponding to the high

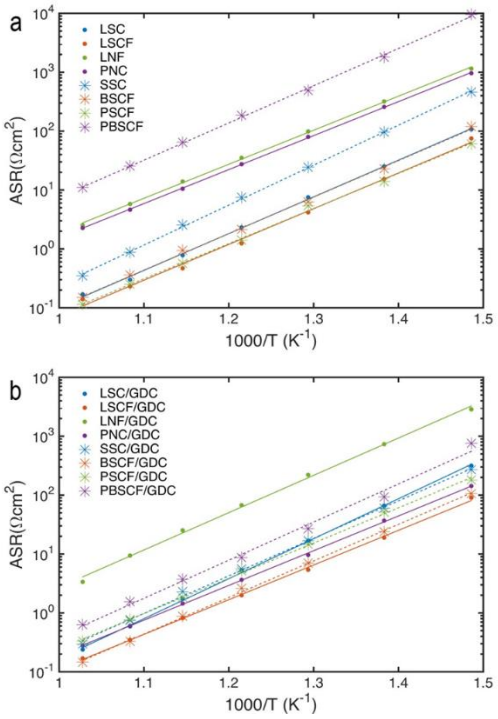

LSC: La-Sr-Co-oxide
LSCF: La-Sr-Co-Fe-oxide
LNF: La-Ni-Fe-oxide
PNC: Pr-Ni-Co-oxide
SSC: Sm-Sr-Co-oxide
BSCF: Ba-Sr-Co-Fe-oxide
PSCF: Pr-Sr-Co-Fe-Oxide
PBSCF: Pr-Ba-Sr-Co-Fe-oxide

GDC: Gd-Ce-oxide

Figure 2: Arrhenius plots of the polarization resistance for single phase cathodes. (b) Arrhenius plots of the polarization resistance for composite cathodes. The activation energies range between 1.15 eV and 1.35 eV.

temperature anneal. Oxygen vacancies are mobile, and they adjust to the frozen concentration of cations. Thus, we still have $\tilde{\mu}_{\ddot{V}_O}(\text{surface}) = \tilde{\mu}_{\ddot{V}_O}(\text{bulk})$ but no longer are the electrochemical potentials of other species equilibrated. Thus, we have $\tilde{\mu}_{Y'_{Zr}}(\text{surface}) \neq \tilde{\mu}_{Y'_{Zr}}(\text{bulk})$. That is, the electrochemical potential of yttrium ions is not equilibrated. Once again, a nonzero space charge potential is determined. Figure 3 shows results under equilibrated and under non-equilibrated conditions. A paper based on this work was published in *J. Electrochem. Soc*. (2017) [17].

II(c):5: Electrochemical Measurements on a Zirconia Sensor at Very Low Temperatures: Many solid oxide electrolytes exhibit high oxygen ion conductivity at elevated temperatures. LSGM, ceria, etc. exhibit higher ionic conductivity than YSZ at a given temperature. At room temperature, YSZ is practically an insulator. However, many measurement instruments have much higher input resistance/impedance than a typical YSZ sample a few mm in dimensions even at room temperature. This suggests it may be possible to make some measurements on YSZ at very low temperatures. In this work, a yttria-stabilized zirconia (YSZ) tube with platinum electrodes was used for the measurement of potential with one electrode exposed to air and the other to H_2-H_2O gas mixtures. Measurements were conducted over a temperature range from 30°C to 475°C using two different meters, one with an input impedance of 10 GΩ and the other with an input impedance > 200 TΩ. With the high impedance meter (electrometer), a voltage of 0.93 V was measured at 30°C, while it was much lower using the low impedance meter. Above ~177°C, readings from both meters converged. From the measurements, the actual cell voltage and the net cell resistance including all polarization resistances were estimated. Above 275°C, the measured voltage was in agreement with the expected Nernst voltage. At lower temperatures, the voltage even with the

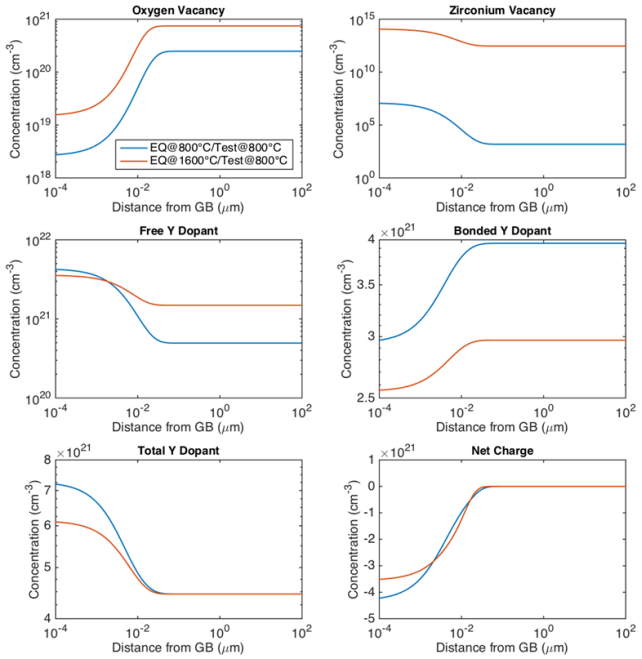

Figure 3: A comparison between defects distribution at equilibrium (blue) and under non-equilibrium conditions (orange). Orange curves represent a sample annealed at 1600^{o}C and quenched to 800^{o}C. Only the oxygen vacancies are mobile. Blue curves represent a sample annealed at 800^{o}C for a very long time to achieve equilibration of all defects (generally not possible at 800^{o}C due to slow cation diffusion). Note both axes are on log-log scale.

electrometer was lower than the calculated Nernst voltage indicating that H_2-H_2O gas phase mixture did not reach equilibrium. Electrochemical impedance spectra (EIS) were obtained. From the EIS spectra, the ohmic resistance was obtained. Above 75^{o}C much of the cell resistance is attributed to electrode polarization. Figure 4(a) shows the measured cell resistance as a function of temperature. The highest measured total cell resistance (which includes ohmic as well as polarization resistances) was ~5 GΩ (at 60^{o}C), while the input impedance of the meter was > 200 TΩ. Figure 4(b) shows potentiometric measurements on the sensor with one side exposed to air and the other to H_2/H_2O mixture. Note the potential could be readily measured near room temperature even with a very high electrode polarization resistance. A paper based on this work was published in the *J. Electrochem. Soc*. (2016) [20].

II(c):6: Measurement of Ionic Conductivity and Electrode Polarization on Pt/YSZ by a DC Technique:
Electrochemical devices such as batteries, fuel cells, and electrolyzers are operated in a DC mode. Electrochemical characterization, however, is typically done using AC methods such as EIS. The objective of this work was to measure ionic conductivity and electrode polarization on a model system by a DC method. The measurement of ionic conductivity and electrode polarization resistance on a 8YSZ sample with platinum paste electrodes was conducted using a DC method with high input impedance meters over a temperature range from 119^{o}C to 589^{o}C. Over the entire temperature range, the meter resistance was much larger than the sample resistance including the polarization resistance. At lower temperatures, a faraday cage was used to minimize noise. The measured polarization resistance was also verified using EIS. The ionic conductivity of 8YSZ exhibited Arrhenius behavior with an activation energy of ~1.1 eV, in good agreement with the literature. In the low current regime, electrode kinetics could be described by the linearized form of the Butler-Volmer equation. At higher current densities, electrode kinetics exhibited

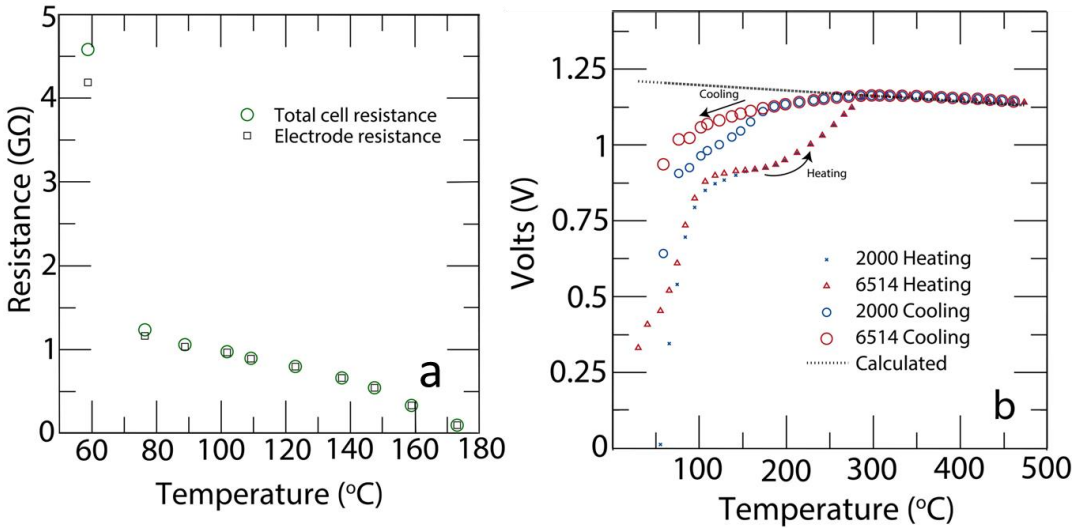

Figure 4: (a) The total cell resistance (circles) obtained from the two meter experiments. The electrode resistance (squares) obtained by subtracting the YSZ tube resistance obtained by EIS measurements from the total cell resistance. The input impedance of the electrometer is > 200 TΩ, which is much greater than ohmic and polarization resistances, thus making reliable measurements possible at near room temperature. (b) Potentiometric measurements using two meters during heating and cooling.

Tafel behavior. The polarization resistance exhibited Arrhenius behavior with the activation energy ranging between 1.05 and 1.27 eV. This work showed that electrode polarization can be investigated using a DC method. Figure 5 shows examples of Tafel plots at two different temperatures. The approach may allow a study of different electrodes in various atmospheres using one sample. A paper based on this work was published in *J. Electrochem. Soc.* (2017) [21].

II(c):7: Effect of Electronic Conductivity on Oxygen Chemical Potential in Oxygen Ion Conductors: Our theoretical work has shown that low level electronic conductivity in predominantly ionic conductors can have a large effect on the chemical potential of the neutral species corresponding to the mobile ion; that is on μ_{O_2} in oxygen ion conductors [7]. Experimental results have also confirmed the consequences of this; namely oxygen electrode delamination in solid oxide electrolysis cells [7]. Laguna-Bercero et al. have actually demonstrated both electrode delamination as well as change in oxygen concentration through the thickness of a YSZ electrolyte –based cell, and the formation of multiple cracks inside the electrolyte [22]. Since YSZ has a very low electronic conductivity [8], a large variation in oxygen concentration was observed (which corresponds to a large variation in μ_{O_2}). We have recently made samples of 8YSZ and samples containing 5% CeO_2 (5Ce8YSZ). CeO_2 was added to one set of samples to increase the electronic conductivity. Both electrodes were LSM + YSZ composites. The discs were heated to 700°C and a DC voltage was applied to pass ~0.2 to ~0.25 Acm^{-2}. After 24 h, the voltage was removed, and the discs were cooled to room temperature. The discs were then examined under an SEM and EDS scans of O, Zr and Y were obtained through the thicknesses of the discs. Figure 6 shows the plots of oxygen concentration across the thicknesses of the two samples. The sample thicknesses were ~1350 microns (YSZ) and ~700 microns (5Ce8YSZ). The changes in oxygen concentration in the discs thus occurred near the electrodes. Experiments will need to be done for a much longer time for composition variation to occur throughout the thicknesses. It is interesting to note that the oxygen concentration in 8YSZ near the positive electrode is ~67% while that near the negative electrode is ~57%. In the middle of the sample the oxygen concentration is ~60%, which is the same as the starting composition. In 5Ce8YSZ, however, there is no enrichment in oxygen near the positive electrode and no depletion near the negative electrode. The

average oxygen concentration is ~62% with some scatter in data (between ~61% and ~64%). The EDS data are not very

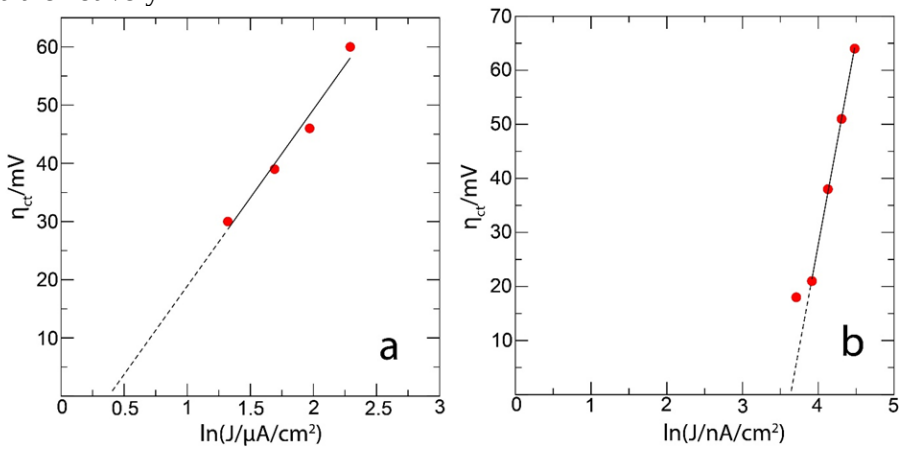

Figure 5: Tafel plots of electrode overpotentials measured using a DC method at (a) 428°C and (b) 268°C. At low temperatures, the typical current density is in nAcm^{-2} range.

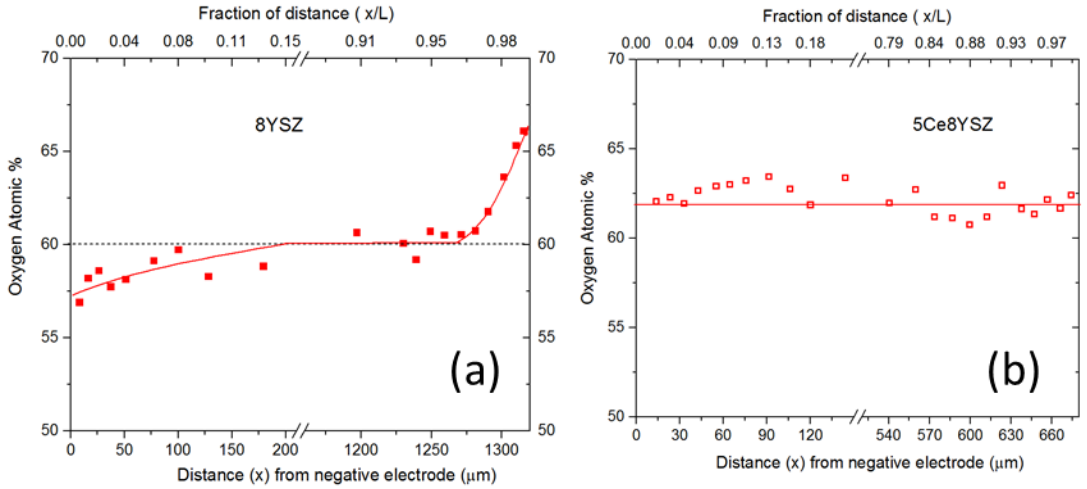

Figure 6: (a) Oxygen concentration profile in 8YSZ after 24h at 700°C under an applied DC voltage. (b) Oxygen concentration profile in 5Ce8YSZ after 24h at 700°C under an applied DC voltage.

accurate. However, the results show that the addition of CeO_2 leads to smoothening of the oxygen concentration. This implies that in 8YSZ, large variations in μ_{O_2} occur through the thickness, but not so in CeO_2-doped samples. A paper based on this work was published in *ECS Trans*. (2017) [23].

II(c):8: Solid Oxide Cells based on Mixed Ionic-Electronic Conducting (MIEC) Electrolytes: Since some level of electronic conductivity is desired in the electrolyte for enhanced stability, an analysis is needed on how to increase stability without compromising performance of an electrochemical device (efficiency of electricity generation – fuel cells, or efficiency of hydrogen generation – electrolysis cells). Theoretical analysis was conducted on reversible cells made with purely ionic conducting electrolyte (8YSZ) and MIEC electrolyte (such as that containing ceria). Figure 7 shows the calculated performance curves for cells with the two types of electrolytes. In the case of the MIEC cell, note that there is a significant electronic current through the cell (lower open circuit voltage than the theoretical value). At the indicated green dots on both sides, the performance levels are identical, the total joule heating is identical, and the efficiency is identical. This theoretical analysis shows that one can in fact use an electrolyte with

significant electronic conductivity. Two 5 cell reversible stacks, one with 8YSZ electrolyte and one with 5Ce8YSZ electrolyte were made by Materials and Systems Research, Inc. and tested at Idaho National Laboratory. The one with

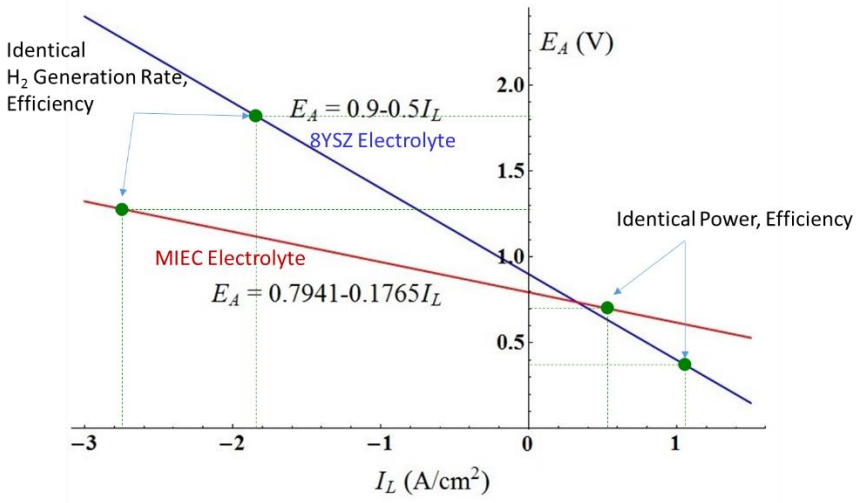

Figure 7: Plots of calculated performance curves for a cell with 8YSZ (blue line) as the electrolyte and an MIEC (red line) electrolyte. For this calculation, the electronic conductivity was assumed to be substantial, ~10% of the ionic conductivity (ionic transference number t_i ~0.9). The green dots on the right side (fuel cell mode) indicate identical performance and efficiency. The green dots on the left side (electrolyzer mode) also indicate identical performance and efficiency.

8YSZ cells exhibited much greater degradation than the one with 5Ce8YSZ cells. A paper based on the theoretical work and stack results was published in *Int. J. Hydrogen Energy* (2015) [24].

II(c):9: EIS Measurements on Proton Exchange Membrane Fuel Cells (PEMFC) with Embedded Ag Screen Probes: Most of the reported measurements have been made on fuel cells across the entire cells using EIS.

Deconvolution of the EIS spectra, however, is often ambiguous. The use of externally placed reference electrodes is also fraught with uncertainties. We have demonstrated that by placing a Pt probe inside a solid electrolyte, local electrochemical potential of electrons, $\tilde{\mu}_e$, can be measured [25,26]. From these measurements, local chemical potential of oxygen, μ_{O_2}, can be determined. However, it is not possible to determine electrode overpotentials using a wire type of probe. It is in concept possible to prepare cells with embedded screen probes such that the geometric areas of the two electrodes (cathode and anode) and the screen probes are the same. The screen probe is contiguous in the metal screen used so that it can be connected to external measuring instruments. At the same time, the electrolyte is also contiguous across the screens. Thus, ionic current can flow through the entire cell, and through the screens. With such cells, it is possible to make EIS measurements across the entire cell, as well as across the screen probes and the two electrodes (cathode and anode) individually. If there is one screen probe, then it is expected that EIS spectra across the anode and the screen, and across the cathode and the screen would allow measurements of electrode polarizations *separately*. The sum of the two sets of spectra should match the EIS spectra obtained across the entire cell. We expect to do these measurements on solid oxide cells in the future. During the current grant period, we conducted the following experiments on PEMFC.

A silver + Nafion solution paste was made. One side of a Nafion membrane was coated with the paste. On top of that, another Nafion membrane was placed. Commercial electrode inks were applied on the two surfaces of the tri-layer structure. A PEM fuel cell was made by sandwiching it between two gas diffusion

layers and was laminated. We have also made PEM fuel cells with a four layer structure which has two screen probes. Here we present some preliminary results with one embedded screen. Figure 8(a) shows a schematic of the PEM fuel cell with an embedded screen. The PEM fuel cell was tested under various conditions. Figure 8(b) shows EIS spectra across the anode and the screen, across the cathode and the

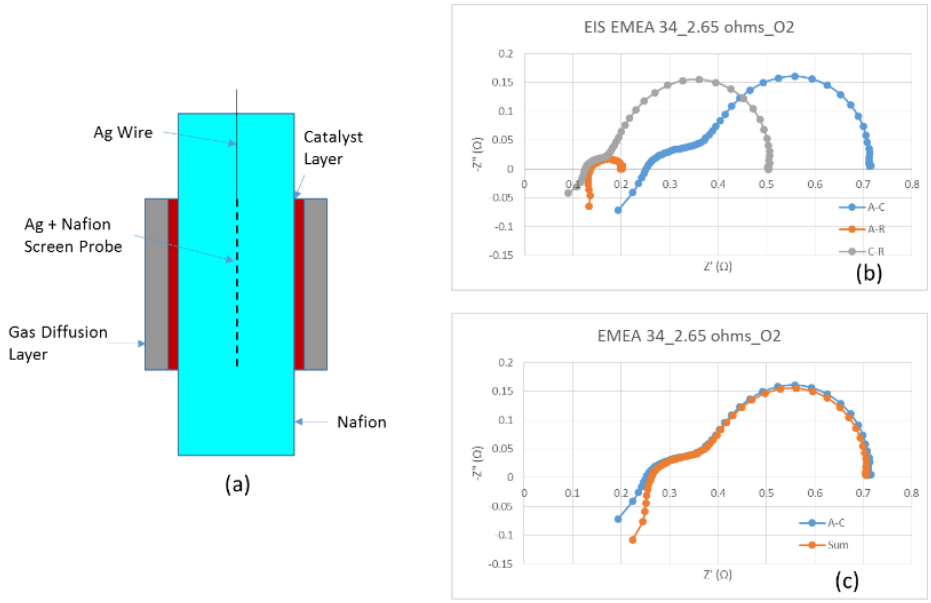

Figure 8: (a) A schematic of a PEM fuel cell with an embedded Ag screen probe. (b) EIS spectra with a DC load of 2.65 Ω across cathode-screen, anode-screen and cathode-anode. (c) EIS spectra across cathode-anode (same as in (b)) and point by point sum of spectra across cathode-screen and anode-screen.

screen, and across the cathode and the anode. Figure 8(c) shows the EIS spectra across the cathode and the anode and a sum of the spectra across the cathode and the screen and across the anode and the screen. As seen from the figure, the sum matches well with spectra measured across the cell. The longer high frequency tail for the sum is due to the inductive tail being included twice in the sum, but only once in the measurements across the cell. Figure 8(b) shows that anode polarization (orange) is much smaller than cathode polarization (gray), which is well known. This work thus demonstrates that separate EIS spectra can be obtained which allows one to separately measure cathode and anode polarizations. A paper based on this work was published in *The J. Electrochem. Soc* (2019). [27]

II(c):10: Carbon Monoxide Poisoning of Platinum by Electrical Resistance Measurements: One of the modes of degradation of PEMC anodes is adsorption of trace levels of CO from the fuel on the anode catalyst thus blocking the active sites where hydrogen oxidation reaction occurs. Carbon monoxide (CO) poisoning of platinum catalysts in proton exchange membrane fuel cells (PEMFC) substantially affects cell performance. Many studies have been reported on performance degradation even with very small concentrations of CO in hydrogen. This work investigated carbon monoxide adsorption/desorption in situ on a 1 nm thick platinum film deposited on a sapphire substrate by measuring the electrical resistance of the film as a function of CO concentration, exposure time and testing temperature. The experimental data showed an increase in film resistance upon exposure to CO containing gases. The film resistance was sensitive to CO exposure at a concentration as low as 1 ppm. A model was developed to determine rate constants and activation energies for CO adsorption/desorption on Pt surface using the measurement of electrical resistance as a function of time. A paper based on this work was published in the *J. Electrochem. Soc.* (2018) [28].

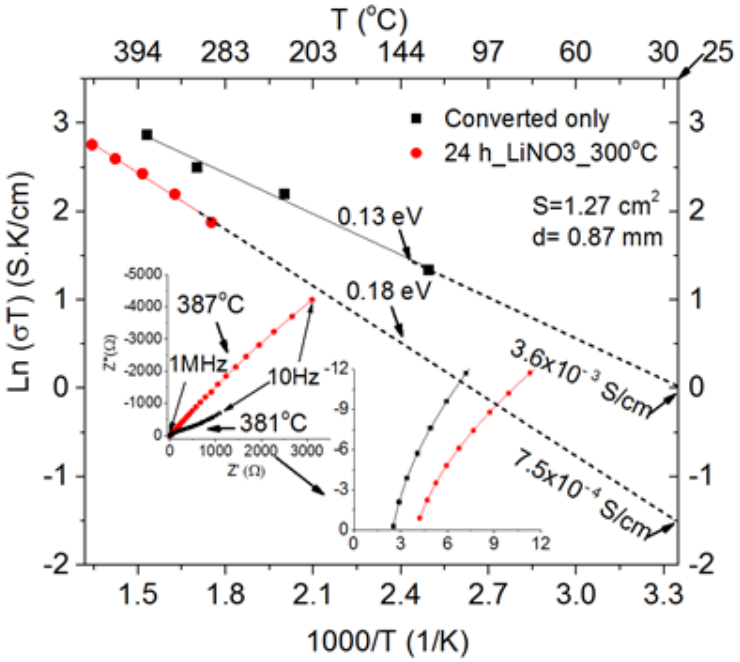

Figure 9: Arrhenius plots of the measured Na^+ ion conductivity on a fully converted sample and after Li^+ ion exchange for 24 h at 300°C.

II(c):11: Synthesis of Li-Ion Conducting Beta"-alumina and a Solid State Lithium Battery: We have conducted preliminary work on the fabrication of Li-ion conducting beta"-alumina and have demonstrated a room temperature solid state battery. Na-beta"-alumina + YSZ composite discs were fabricated by vapor phase conversion of sintered alumina + YSZ discs. These were then ion-exchanged in molten $LiNO_3$ to replace Na^+ by Li^+. Figure 9 shows the measured ionic conductivities of Na-beta"-alumina + YSZ and Li-beta"-alumina + YSZ. Lithium ion conductivity is lower than that of Na-beta"-alumina, but is still quite high and comparable to some other lithium ion conductors. At low temperatures, oxygen ion conductivity of YSZ is much lower than that for alkali ion. A solid state lithium battery was demonstrated. A paper based on this work was published in *ECS Transactions* (2017) [29].

References

1. D. Kondepudi and I. Prigogine, 'Modern Thermodynamics: From Heat Engines to Dissipative Structures', John Wiley and Sons, (2000).
2. R. Haase, 'Thermodynamics of Irreversible Processes', Dover Publications, New York, (1990).
3. S. Kjelstrup and D. Bedeaux, 'Non-Equilibrium Thermodynamics of Heterogeneous Systems', World Scientific (2008).
4. A. V. Virkar, 'Theoretical analysis of the role of interfaces in transport through oxygen ion and electron conducting membranes', *J. Power Sources*, **147** 8-31 (2005).
5. A. V. Virkar, 'Transport through mixed proton, oxygen ion and electron/hole conductors: Analysis of fuel cells and electrolyzers using Onsager equations', *Int. J. Hydrogen Energy*, **37** 12609-12628 (2012).
6. A. V. Virkar, 'A model for degradation of electrochemical devices based on linear non-equilibrium thermodynamics and its application to lithium ion batteries', *J. Power Sources*, **196** 5970-5984 (2011).
7. A. V. Virkar, 'Mechanism of oxygen electrode delamination in solid oxide electrolyzer cells', *Int. J. Hyd. Energy*, **35** 9527-9543 (2010).
8. J. H. Park and R. Blumenthal, 'Electronic transport in 8 mole percent Y_2O_3-ZrO_2', J. Electrochem. Soc., 136 2867-2876 (1989).

9. K. Kobayashi, Y. Kai, S. Yamaguchi, N. Fukatsu, T. Kawashima and Y. Iguchi, 'Electronic conductivity measurements of 5% TiO_2-doped YSZ by a d. c. polarization technique', *Solid State Ionics,* **93** [3-4] 193-199 (1997).
10. M. H. Hebb, 'Electrical conductivity of silver sulfide', *J. Chem. Phys.,* **20** 185-190 (1952).
11. C. Wagner, 'Galvanic cells with solid electrolytes involving ionic and electronic conduction', Proc. 7th International Conference Electrochem. Thermodyn. Kinetics, p.361-377 Lindau (1955).
12. L. Zhu, L. Zhang and A. V. Virkar, 'Measurement of Ionic and Electronic Conductivities of Yttria-Stabilized Zirconia by an Embedded Electrode Method', *J. Electrochem. Soc.,* **161** (3) F298-F309 (2015).
13. L. Zhang, L. Zhu and A. V. Virkar, 'Electronic conductivity measurement of yttria-stabilized zirconia solid electrolytes by a transient technique', *J. Power Sources,* **302** 98-106 (2016).
14. X. Guo, 'Physical origin of the intrinsic grain-boundary resistivity of stabilized-zirconia: Role of the space-charge layers', *Solid State Ionics,* **81** 235-242 (1995).
15. X. Guo and J. Maier, 'Grain Boundary Blocking Effect in Zirconia: A Schottky Barrier Analysis', *J. Electrochem. Soc.,* **148** (3) E121-E126 (2001).
16. K. L. Kliewer and J. S. Koehler, 'Space Charge in Ionic Crystals. I. General Approach with Application to NaCl', *Phys. Rev.,* **140** 4A, A1226-A1240 (1965).
17. L. Zhang and A. V. Virkar, 'On Space Charge and Spatial Distribution of Defects in Yttria-Stabilized Zirconia', *J. Electrochem. Soc.,* **164** (3) F1506-F1523 (2017).
18. L. Zhu, L. Zhang and A. V. Virkar, 'A parametric model for solid oxide fuel cells based on measurements made on cell materials and components', *J. Power Sources,* **291** 138155 (2015).
19. L. Zhang, L. Zhu and A. V. Virkar, 'Nanostructured Cathodes for Solid Oxide Fuel Cells by a Solution Spary-Coating Process', L. Zhang, L. Zhu and A. V. Virkar, J. Electrcohem. Soc., 163 (5) F1358-F1365 (2016).
20. A. Szendrei, T. D. Sparks and A. V. Virkar, 'Use of Yttria-Stabilzied Zirconia for Potentiometric Measurements at Low Temperatures', *J. Electrochem. Soc.,* **163** (5) F416-F420 (2016).
21. A. Szendrei, T. D. Sparks and A. V. Virkar, 'Measurement of Ionic Conductivity and Electrode Polarization at Low Temperatures on 8YSZ by a DC Technique', *J. Electrochem. Soc.,* 164 (14) F1543-F1550 (2017).
22. M. A. Laguna-Bercero, R. Campana, A. Larrea, J. A. Kilner, and V. M. Orera, 'Electrolyte degradation in anode-supported microtubular yttria-stabilzied zirconia based solid oxide steam electrolysis cells at high voltages of operation', *J. Power Sources,* **196** 8942-8947 (2011).
23. L. Zhu, L. Zhang and A. V. Virkar, 'Role of Electronic Conductivity in Stability of Solid Oxide Electroyzer Cells', *ECS Transactions,* **80** (9) 81-89 (2017).
24. A. V. Virkar and G. Tao, 'Reversible high temperature cells for power generation and hydrogen production using mixed ionic-electronic conducting solid electrolytes', *Int. J. Hyd. Energy,* **40** 5561-5577 (2015).
25. H-T. Lim and A. V. Virkar, 'Measurement of oxygen chemical potential in thin electrolyte film, anode-supported solid oxide fuel cells', *J. Power Sources,* **180** [1] 92-102 (2008).
26. H-T. Lim and A. V. Virkar, 'Measurement of oxygen chemical potential in Gd_2O_3-doped ceria-Y_2O_3-stabilized zirconia bi-layer electrolyte, anode supported solid oxide fuel cells', *J. Power Sources,* **192** [2] 267-278 (2009).
27. A. Szendrei, T. D. Sparks and A. V. Virkar, 'Thre and Four-Electrode Electrochemical Impedance Spectroscopy Studies using Embedded Composite Thin Film Pseudo-Reference Electrodes in Proton Exchange Membrane Fuel Cells', *J. Electrochem. Soc.,* **166** (12) F784-F795 (2019).
28. L. Zhu, L. Zhang and A. V. Virkar, 'A study of CO Adsorption/Desorption on a Thin Platinum Film by the Measurement of Electrical Resistance', *J. Electrochem. Soc.,* **165** (3) F232-F237 (2018).
29. L. Zhu and A. V. Virkar, 'Fabrication of Li-β"-Alumina + Yttria-Stabilzied Zirconia Composites and Their Application in Lithium Battery', *ECS Transactions,* **80** (9) 35-44 (2017).